32nd URSI GASS, Montreal, 19–26 August 2017

Displacement-Current Phase Tomography and Electrical Capacitance Tomography for Air-Water Flow Systems

Cagdas Gunes*(1), Shah Chowdhury(1), Qussai M. Marashdeh(2) and Fernando L. Teixeira(1)
(1) ElectroScience Laboratory, Department of Electrical and Computer Engineering,
Ohio State University, Columbus, OH 43212 USA
(2) Tech4Imaging LLC, Columbus, OH 43220 USA

Abstract

Electrical Capacitance Tomography (ECT) is an imaging modality for spatial reconstruction of the dielectric permittivity distribution inside a region of interest (RoI). ECT utilizes mutual capacitance measurements obtained from electrode sensor pairs placed on a dielectric vessel surrounding the RoI. Displacement-Current Phase Tomography (DCPT) is a variant technique based on the phase information of capacitance measurements enabled by the same harware as ECT. DCPT is predicated on having the sensor plates excited by time-harmonic signals in the quasi-static regime, as commonly done in ECT. Under the presence of lossy media in the RoI, it can be shown that DCPT has an extended linear range (versus ECT) for the dependency between the measurement data and the spatial distribution. This result, together with the fact that no electrical contact is necessary unlike electrical impedance tomography (EIT), makes DCPT, either separately or in combination with ECT, a suitable modality for the reconstruction of lossy media distributions. In this summary paper, we present a comparison between DCPT and ECT results for the imaging of air-water flow sytems.

1 Introduction

Electrical capacitance tomography (ECT) is a low-cost, lightweight, and noninvasive imaging modality suited for obtaining a cross-sectional image of a region of interest (RoI) by means of non-contact electrodes placed around it [1, 2, 3]. Due to its relatively fast acquisition speeds, ECT is widely applied for real-time monitoring of multi-phase flows and industrial processes [4, 10, 6, 7].

The relation between the measured mutual capacitance C and the permittivity distribution $\varepsilon(x,y)$ for an ECT system is governed by the equation [9]:

$$C = \frac{Q}{V} = -\frac{1}{V}\iint_S \varepsilon(x,y)\nabla\phi(x,y)\cdot\hat{n}dS \qquad (1)$$

where V is the applied voltage on one of the electrodes while the others remain grounded, $\phi(x,y)$ is the resulting electric potential in the RoI, $\hat{n}$ is a unit vector normal to the electrode, and the surface integral is performed over the electrode area S. The capacitance depends nonlinearly on $\varepsilon(x,y)$ since $\phi(x,y)$ is affected by $\varepsilon(x,y)$. A traditional approach to linearize this dependence is to use the Born approximation [8], which is valid for small perturbations on $\varepsilon(x,y)$. With this assumption, and after a discretization of the RoI into pixels, the relation between measured capacitance and permittivity distribution can be approximated via a sensitivity matrix [11].

Displacement-current phase tomography (DCPT) is a variant imaging technique based on the same basic hardware setup as ECT yet utilizing the inherent phase information on displacement current between sensing electrodes excited by time-harmonic voltages [12, 13, 14]. In contrast to ECT, DCPT is sensitive to medium losses in the RoI. One attractive feature of DCPT is its extended range of linear behaviour for the dependency between the measurement data and the material distribution, as compared to ECT [12]. These features makes DCPT more suitable for imaging of flow systems with losses and more significant material differences, like air-water flow systems.

2 DCPT Reconstruction

DCPT formulation starts from the energy relations between sensing electrodes where each sensing pair can be considered as a two terminal system. The complex admittance Y between the terminals of this system can be written as

$$Y = \frac{P_c^*}{|V|^2/2} = \frac{2}{|V|^2}[\langle P_d\rangle - j2\omega(\langle W_m\rangle - \langle W_e\rangle)]. \qquad (2)$$

where P_c is the complex power (the imaginary part being the reactive power), P_d is the energy dissipated by the material distribution inside the RoI, ω is the angular frequency and W_m, W_e are the (average) energy stored in the magnetic and electric fields respectively (note that these stored energy terms also include damping losses [15]). In the quasi-static frequency regime, magnetic effects are negligible and all the loss factors can be grouped as $\gamma \equiv \sigma + \omega\varepsilon''$ where σ is the conductivity and ε'' is strictly the dielectric loss [16]. The phase of the admittance between the electrode plates can be expressed as

$$\varphi = \pi/2 - \tan^{-1}\left(\frac{\int_{\mathscr{V}}\gamma|\vec{E}|^2\,dv}{\int_{\mathscr{V}}\omega\varepsilon'|\vec{E}|^2\,dv}\right) \qquad (3)$$

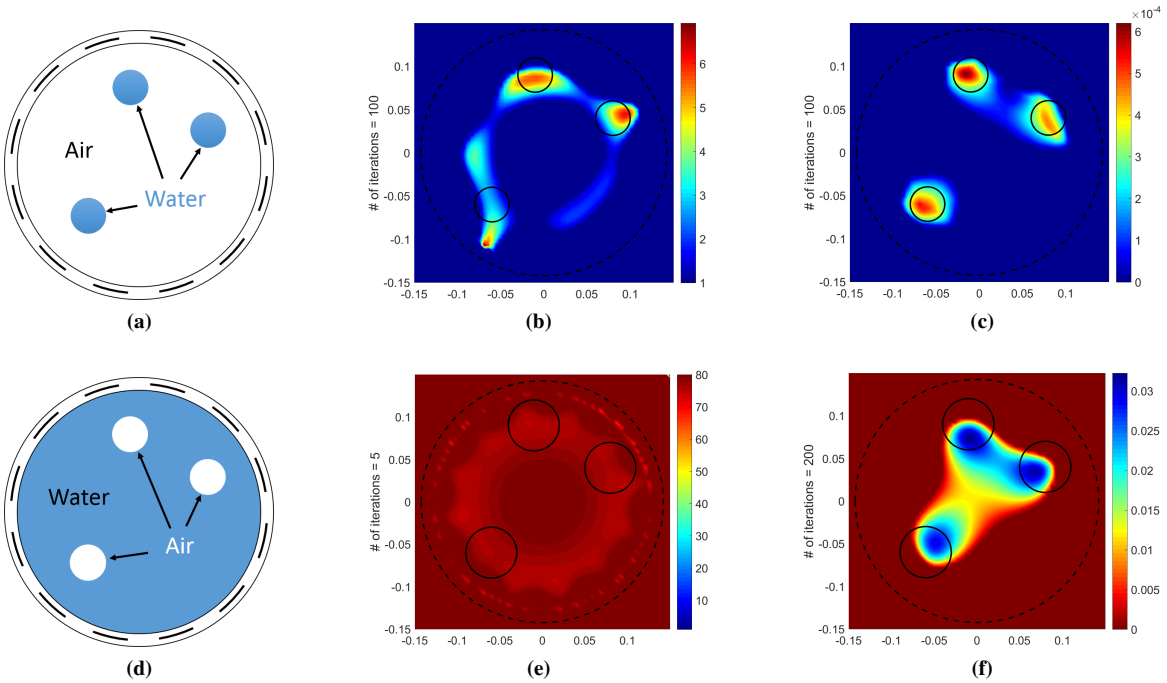

Figure 1. Comparison of ECT and DCPT image reconstruction results. (a) Water-in-air flow. (b) ECT water-in-air results. (c) DCPT water-in air results. (d) Air-in-water flow. (e) ECT air-in-water results. (f) DCPT air-in-water results.

where ε' and $\vec{E}$ are the dielectric permittivity and electric field values inside the RoI volume $\mathscr{V}$. If the RoI is filled with air, $\varphi = \pi/2$. For small losses in the RoI, φ is a small angle. DCPT operates in the regime where the loss-tangent is small, so that the tangent factor in the above equation can be approximated by its argument. From this point on, the conventional Born approximation can be used similarly to ECT. This allows both methods to employ the same sensitivity matrix. The small loss-tangent assumption is a limiting factor for DCPT applications: if losses are not small, then the reconstruction will not be accurate. Another limitation for DCPT is the selection of the operating frequency for a given material conductivity distribution inside RoI. If the frequency selected is too high, skin-depth effects may start to play a role and the imaging will not be accurate.

3 Simulation Results and Discussion

Air-in-water and water-in-air flow systems are considered as case studies. Simulations are performed on a cylindrical domain of 0.15 m radius surrounded by twelve electrodes. The gap between neighbor electrodes comprise 20% of their length. Three circular objects with radius of 0.03 m are placed at various locations inside the RoI as shown in Figure. 1-(a),(d). The forward simulation to obtain mutual capacitances is performed at 300 kHz on COMSOL^{TM} software. The image reconstructions are done on MATLAB^{TM} considering the RoI discretized by 64×64 pixels. The locations of the objects are indicated by black circles in Figure 1. Tap water is considered with relative permittivity $\varepsilon = 80$ and conductivity σ =0.05 S/m. The reconstructed images are obtained using the Landweber algorithm with optimal step length [17] after following the appropriate normalization schemes. A projection filter is used for regularization [18]. The number of iterations required for each of these images are shown next to each plot. The choice for the iteration number is done empirically as the Landweber method has a semi-convergence property [19]. And all the images are interpolated from the reconstructed pixel distribution. The center column results in Figure 1 show ECT images. The right column of Figure 1 shows DCPT images. The DCPT results shown in Figure 1(c) provide a slightly better location prediction for the objects location than the ECT results shown in Figure 1(b). The case of air bubbles in water is more challenging because of the high permittivity of water. In this case, the ECT results shown in Figure. 1(e) cannot detect the air bubbles inside the ROI. For the same case, DCPT shows a better performance as seen in Figure. 1(f).

4 Acknowledgements

This work was supported by the National Aeronautics and Space Administration (NASA) under grant NNX16CC10C.

References

[1] S. Huang, A. Plaskowski, C. Xie, and M. Beck, "Capacitance-based tomographic flow imaging system," *Electron. Lett.*, vol. 24, no. 7, pp. 418-419, Mar 1988, doi: 10.1049/el:19880283.

[2] C.G. Xie, A.L. Stott, A. Plaskowski, and M.S. Beck, "Design of capacitance electrodes for concentration

measurement of two-phase flow," *EMeasurement Science and Technology*, vol. 1, no. 1, p. 65, 1990, doi: 10.1109/ICSENS.2016.7808640.

[3] Q. Marashdeh, F. L. Teixeira, and L.-S. Fan, "Electrical capacitance tomography," in *Industrial Tomography: Systems and Applications*, 1st ed., M. Wang, Ed. Cambridge, UK: Woodhead/Elsevier, 2015, ch. 1, pp. 3–21, isbn: 9781782421238.

[4] Q. Marashdeh, W. Warsito, L.-S. Fan, and F. L. Teixeira, "A nonlinear image reconstruction technique for ECT using combined neural network approach," *Meas. Sci. Technol.*, vol. 17, no. 8, pp. 2097-2103, 2006, doi: 10.1088/0957-0233/17/8/007.

[5] K.-J. Alme and S. Mylvaganam, "Electrical capacitance tomography: Sensor models, design, simulations, and experimental verification," *IEEE Sensors J.*, **6**, 5, may 2006, pp. 1256–1266, doi:10.1109/JSEN.2006.881409.

[6] Q. Marashdeh, W. Warsito, L.-S. Fan, and F. L. Teixeira, "A multimodal tomography system based on ECT sensors," *IEEE Sensors J.*, **7**, 3, March 2007, pp. 426–433. doi:10.1109/JSEN.2006.890149.

[7] A. Wang, Q. Marashdeh, F. L. Teixeira, and L. S. Fan, "Electrical capacitance volume tomography: A comparison betwen 12- and 24-channel sensor systems," *Prog. Electromag. Res.*, **41**, February 2015, pp. 73–84, doi:10.2528/PIERM15011412.

[8] W. C. Chew, *Waves and Field In Inhomogeneous Media*, IEEE Press, Piscataway, NJ, 1995.

[9] Z. Zeeshan, F. L. Teixeira, and Q. Marashdeh, "Sensitivity map computation in adaptive electrical capacitance volume tomography with multielectrode excitations," *Electron. Lett.*, **51**, 4, February 2015, pp. 334–336, doi:10.1049/el.2014.3855.

[10] K. J. Alme and S. Mylvaganam, "Electrical capacitance tomography - sensor models, design, simulations, and experimental verification," *IEEE Sensors J.*, **6**, 5, September 2006, pp. 1256-1266, doi: 10.1109/JSEN.2006.881409.

[11] Q.M. Marashdeh and F.L. Teixeira, "Sensitivity matrix calculation for fast 3-D electrical capacitance tomography (ECT) of flow systems," *EEE Trans. Magn.*, **40**, 2, February 2004, pp. 1204-1207, doi: 10.1109/TMAG.2004.825039.

[12] C. Gunes, Q. M. Marashdeh, and F. L. Teixeira, "A Comparison Between Electrical Capacitance Tomography and Displacement-Current Phase Tomography," submitted, 2016.

[13] A. V. Korjenevsky, "Electric field tomography for contactless imaging of resistivity in biomedical applications," *Physiol. Meas.*, **25**, February 2004, pp. 391-401, doi: 10.1088/0967-3334/25/1/042.

[14] A. V. Korjenevsky and T. S. Tuykin, "Phase measurement for electric field tomography," *Physiol. Meas.*, **29**, pp. S151-S161, June 2008, doi: 10.1088/0967-3334/29/6/S13.

[15] D. T. Paris and F. K. Hurd, *Basic Electromagnetic Theory*, McGraw-Hill, New York,1969.

[16] C. A. Levis, J. T. Johnson, and F. L. Teixeira, *Radiowave Propagation: Physics and Applications*, John Wiley & Sons, New York, 2010.

[17] S. Liu, L. Fu and W.Q. Yang "Optimization of an iterative image reconstruction algorithm for electrical capacitance tomography," *Meas. Sci. Technol.*, **10**, 7, June 1999, L37–L39, doi: 10.1088/0957-0233/10/7/102.

[18] J. D. Jang ,S. H. Lee, K. Y. Kim, and B. Y. Choi, "Modified iterative Landweber method in electrical capacitance tomography," *Meas. Sci. Technol.*, **17**, 7, July 2006, pp. 1909-1917, doi: 10.1088/0957-0233/17/7/032.

[19] W. Q. Yang and L. H. Peng, "Image reconstruction algorithms for electrical capacitance tomography," *Meas. Sci. Technol.*, **14**, 1, January 2003, pp. R1–R13, doi: 10.1088/0957-0233/14/1/201.